

Simulations of Membrane-Disrupting Peptides II: AMP Piscidin 1 Favors Surface Defects over Pores

B. Scott Perrin, Jr.,¹ Riqiang Fu,² Myriam L. Cotten,³ and Richard W. Pastor^{1,*}

¹Laboratory of Computational Biology, National Heart, Lung, and Blood Institute, National Institutes of Health, Bethesda, Maryland; ²National High Magnetic Field Laboratory, Tallahassee, Florida; and ³Department of Applied Science, The College of William & Mary, Williamsburg, Virginia

ABSTRACT Antimicrobial peptides (AMPs) that disrupt bacterial membranes are promising therapeutics against the growing number of antibiotic-resistant bacteria. The mechanism of membrane disruption by the AMP piscidin 1 was examined with multimicrosecond all-atom molecular dynamics simulations and solid-state NMR spectroscopy. The primary simulation was initialized with 20 peptides in four barrel-stave pores in a fully hydrated 1-palmitoyl-2-oleoyl-*sn*-glycero-3-phosphocholine/1-palmitoyl-2-oleoyl-*sn*-glycero-3-phosphoglycerol bilayer. The four pores relaxed to toroidal by 200 ns, only one porelike structure containing two transmembrane helices remained at 26 μ s, and none of the 18 peptides released to the surface reinserted to form pores. The simulation was repeated at 413 K with an applied electric field and all peptides were surface-bound by 200 ns. Trajectories of surface-bound piscidin with and without applied fields at 313 and 413 K and totaling 6 μ s show transient distortions of the bilayer/water interface (consistent with ³¹P NMR), but no insertion to transmembrane or pore states. ¹⁵N chemical shifts confirm a fully surface-bound conformation. Taken together, the simulation and experimental results imply that transient defects rather than stable pores are responsible for membrane disruption by piscidin 1, and likely other AMPs.

INTRODUCTION

Antimicrobial peptides (AMPs) are promising guides in the design of novel therapeutics due to their broad-spectrum activity, rapid eradication of their targets, and low incidence of induced bacterial resistance (1). AMPs are generally <50 residues in length, cover a broad range of amphipathic secondary structures, and have a host of proposed mechanisms. Of particular interest are cationic amphipathic α -helices that function by adsorbing onto anionic membranes of bacterial cells where they fold, aggregate, and disrupt the membrane as detected by destabilizing permeabilization and/or membrane lysis (2). Some AMPs may also have roles inhibiting intracellular targets (3,4). While the disruption mechanisms of AMPs are still unknown (5), the toroidal pore model developed for melittin, a peptide toxin in the venom secreted by bees, has been postulated based on shared physicochemical properties (e.g., amphipathicity, length, secondary structure) (6). This study tests the toroidal pore model using multimicrosecond simulations and solid-state NMR (ssNMR) spectroscopy of the antimicrobial peptide piscidin

1 (p1) in bilayers of the bacterial-cell mimic 3:1 1-palmitoyl-2-oleoyl-*sn*-glycero-3-phosphocholine (POPC)/1-palmitoyl-2-oleoyl-*sn*-glycero-3-phosphoglycerol (POPG) at full hydration. This is a continuation of the preceding article (denoted “Article I”) that demonstrated stability of an alamethicin pore over the course of a 14 μ s trajectory. The remainder of this Introduction presents additional background on membrane disruption by peptides, p1 in particular, and the relevant methods. It closes with an outline of the article.

Models for membrane disruption fall into two categories: pore and nonpore. The simplest pore is barrel-stave, in which a number of transmembrane peptides pack with their hydrophilic surfaces aligned toward the center of the water-filled pore (like staves of a barrel). Peptides forming barrel-stave pores have relatively small fractions of hydrophilic to hydrophobic areas (the so-called polar angle when the peptides are modeled as α -helices). Examples of well-characterized barrel-stave pores include alamethicin (7–11) (the subject of Article I) and dermicidin (12). When the hydrophobic and hydrophilic areas are approximately equal (a polar angle near 180°) the tight packing of a barrel-stave pore is destabilized by simple geometric considerations; i.e., there is too little hydrophobic surface area to pack favorably

Submitted June 24, 2016, and accepted for publication August 10, 2016.

*Correspondence: pastorr@nhlbi.nih.gov

Editor: Scott Feller.

<http://dx.doi.org/10.1016/j.bpj.2016.08.015>

with undistorted lipid chains (13). This imbalance causes the peptides to tilt with respect to the bilayer normal and to recruit lipid headgroups to the interior of the membrane to form what is termed a “toroidal pore”. The resulting lipid distortion is evident from ^{31}P chemical shifts of oriented samples in ssNMR (14). Melittin is the most studied example of a toroidal pore (6,15,16). A subclass, disordered toroidal pores, has been proposed to include pores where peptides with a range of orientations coexist (17), but for the purposes of this study toroidal and disordered toroidal pores are grouped, and distinguished from barrel-stave. The polar angle of most AMPs is near 180° , which is expected to favor a toroidal over a barrel-stave pore (13). However, while ssNMR measurements of ^{15}N -labeled peptides clearly indicate that pores of toxins and peptaibols are in transmembrane (TM) orientations, host-defense AMPs appear to be predominantly surface-bound (S) or highly tilted (T) when associated with membranes (18); see sketch in Fig. S1 in the Supporting Material for definitions of these orientations. Furthermore, dye leakage measurements of many (but not all) AMPs are not consistent with stable pores (19). Rather, leakage from dye-filled liposomes occurs in bursts immediately after addition of the peptide, and then stops. The leakage can be restarted by addition of more peptide, but is not continuous as would be expected from a sizable population of stable pores.

The preceding considerations have motivated a range of nonpore mechanisms for AMP membrane disruption. These models range from simple thinning (which makes the membrane more permeable) to membrane remodeling, and include several named models: charge-clustering (aggregates of anionic lipids around cationic AMPs) (20); interfacial activity (rearrangement of the polar and nonpolar lipid groups generated by the imperfect amphipathicity of surface-bound AMP) (21); and detergent/carpet (destabilization of the lamellar structure of the bilayer and formation of micelles or vesicles) (22,23). The structures associated with most nonpore models are probably best described as transient defects. These defects will have some porelike features, but they are difficult to characterize because of their intrinsic disorder and short lifetimes.

Piscidin 1 (FFHHIFRGIVHVGKTIHRLVTG) is an AMP with strong antimicrobial activity and a well-characterized surface-bound structure, but an undefined active state. The peptide exhibits antimicrobial activity against methicillin-resistant *Staphylococcus aureus* (24), viruses such as HIV-1 (25), fungi (26), and cancer cells (27). Like other AMPs, piscidin induces dye leakage in model membranes and membrane disruption is proposed to be its primary mechanism of action against bacteria (28,29). The surface-bound structures of p1 were determined independently by ssNMR and all-atom molecular dynamics (MD) in two different bacterial cell mimics (30). Both methods yielded highly helical structures parallel to the membrane surface, and a $20\text{--}30^\circ$ kink about the helical axis. Subsequent MD

simulations demonstrated membrane thinning and induction of positive spontaneous curvature by p1 in 3:1 POPC/POPG bilayers (31). Experimental evidence for toroidal pores in bilayers with p1 comes from conductance (28) and dye leakage measurements (26,29); evidence of a carpet mechanism leading to toroidal pores was inferred from ssNMR investigations in bicelles (32). However, no porelike structure has been characterized.

The initial steps to membrane disruption (inserting and folding on the membrane surface) followed by aggregation, insertion, and possible pore formation take microseconds to minutes (33). While all-atom MD simulations are an ideal method for determining the forces involved in the disruption of membranes by amphipathic peptides, it is difficult to achieve timescales longer than several microseconds on conventional computers. Fortunately, special-purpose computers, such as Anton (34), greatly enhance the speed of all-atom MD simulations, and make multimicrosecond timescales accessible. For example, Article I presents a $14\text{-}\mu\text{s}$ trajectory of a six-peptide alamethicin pore in DOPC to demonstrate the stability when using the CHARMM36 lipid and protein parameters (35). Additionally, a four-peptide melittin pore simulated on Anton started in a barrel-stave arrangement quickly became toroidal and remained stable for the duration of the $9\text{-}\mu\text{s}$ trajectory (15). These results, which agree with experimental data, support the notion that a similar simulation protocol can be used to assess the stability of AMP pores.

The first two subsections of the Results and Discussion report a $26\ \mu\text{s}$ trajectory of 20 transmembrane p1 in four pores, and a $2.5\ \mu\text{s}$ trajectory initialized from 16 surface-bound p1; both simulations were carried out in 3:1 POPC/POPG and a peptide/lipid ratio of 1:20 (the same as previous ssNMR measurements (30)) at 313 K with no external electric field. Peptide and lipid orientations in the simulations are then compared to orientations measured by ssNMR at three different temperatures (278, 285, and 305 K). The simulations are repeated at 413 K and with a $-0.2\ \text{V}$ electric field (the same conditions that induced insertion of the antibiotic peptide alamethicin in Article I (35)). The characteristics of the p1 S-orientation are compared to the current nonpore mechanisms of membrane disruption, and differences with alamethicin are considered.

MATERIALS AND METHODS

All simulations were performed with a constant number of atoms, pressure, and temperature (i.e., NPT). The equations of motion were determined from the Verlet algorithm with a time step of 2.0 fs. The Lennard-Jones potentials were terminated at $12\ \text{Å}$, with a smoothing function operating between 8 and $12\ \text{Å}$. Simulations were performed in a tetragonal unit cell with x - and y dimensions set to the same length and independent of the z dimension. The temperature was maintained at 313 K by the Nosé-Hoover thermostat (36,37). A total pressure of 1 atm was maintained by a Nosé-Hoover piston (38,39) (using CHARMM; 40) or the Martyna-Tobias-Klein barostat (41) with semiisotropic scaling applied every 100 time steps (using the Anton

supercomputer; D. E. Shaw Research, New York City, NY). Long-range interactions were evaluated every time step for simulations run with CHARMM and every other time step for those run on Anton.

CHARMM 38b2 (40) and the National Heart, Lung and Blood Institute LoBoS cluster were used for the preparation of simulations run on Anton (Anton requires starting trajectories with well-equilibrated velocities), the full surface-bound simulations, and analysis of all simulations. CHARMM 36 protein (42) and lipid (43) parameters with modified Lennard-Jones pairwise distances for sodium ions interacting with select lipid oxygens (44) were used in all simulations. The systems were solvated with TIP3P water. Initial conditions for all simulations were generated with CHARMM-GUI (45), and the details are given below.

Piscidin pore simulations

Twenty p1 peptides were built as ideal α -helices with extended side chains, and the helical axes aligned along z . The peptides were centered at $z = 0$ and with their helical axis along the perimeter of the pore. Peptides were translated to form four pores, each with a radius of 20 Å. The peptides were then rotated around the helical axis so that hydrophilic side chains faced the center of the pore. Two of the pores contained six peptides, while the other two contain four. For one 6-peptide and one 4-peptide pore, alternating peptides were rotated to align the peptides in an antiparallel orientation. Both parallel and antiparallel barrel-stave peptide pores have been crystallized (alamethicin (46) and dermicidin (12), respectively), therefore these structures guided the assembly of the piscidin pores using peptides aligned parallel or antiparallel with respect to each other in each pore. Four pores were evenly separated in the simulation, with the center of the pores ~63 Å apart. A quantity of 300 POPCs and 100 POPGs were packed into a bilayer around the pores. Each leaflet was initialized with 150 POPCs and 50 POPGs. The simulation had a tetragonal unit cell with dimensions of 126.3×126.3 Å along the x - and y directions. A quantity of 25,542 water molecules was added to reach a cell height (z) of 85.0 Å to meet the requirement of a minimum ratio of 1.5 between the longest and smallest dimensions for Anton. Twenty sodium ions were required to neutralize the system. A 0.1 M salt concentration was set by adding 56 sodium and 56 more chloride ions. The system was replicated in all three dimensions by P1 boundary conditions. The simulation was run for 100 ns on LoBoS and then transferred to Anton and run for 26 μ s. Eight replica simulations were started after 25 μ s on Anton to test the stability of the remaining pore. Three were replicas with the same conditions, but new velocities. The remaining three had different combinations of temperatures (313 or 413 K) and applied electric field strengths (0.0, ± 0.2). (Relevant information for all of the simulations is included in Table 1.)

Simulating a single large bilayer with four pores as opposed to four smaller bilayers with one pore each decreases the influence of leaflet imbalance as lipids and peptides join the pore or surface, reduces the effects of periodic boundary conditions, and provides a reservoir of surface-bound peptides to potentially reincorporate into the pores after peptides transition to the surface.

Surface-bound, full hydration simulations

Eight p1 peptides were built as ideal α -helices with extended side chains and the helical axes aligned along the xy plane. The peptides were rotated around the helical axis so that hydrophobic residues faced the negative z direction (toward the bilayer interior) and hydrophilic residues faced the positive z direction. The peptides were translated 14 Å in the $+z$ direction and along the xy plane to equally separate the peptides. A similar set of eight peptides was set up on the xy plane at -14 Å, with hydrophobic residues in the positive z direction and hydrophilic residues in the negative z direction. The bilayer midplane was at $z = 0$ Å. Two-hundred-forty POPCs and 80 POPGs were randomly packed around the peptides with acyl chains between the planes of $z = 14$ Å and $z = -14$ Å. Each leaflet had 120 POPCs and 40 POPGs. This simulation had the same peptide/lipid (1:20) as the 20 μ s simulation. The system was solvated with 17,948 waters, 80 sodiums, and 74 chlorides. The simulation was run for 2.5 μ s on LoBoS.

In a second set of surface-bound simulations, 10 piscidin peptides were assembled with their centers of mass at $z = 14$ Å and their helical axes parallel to the membrane normal. Three-hundred POPC and one-hundred POPG were randomly packed around the peptides with acyl chains between the planes of $z = 14$ Å and $z = -14$ Å, with 180 lipids on the same leaflet as the peptides and 220 lipids on the opposing leaflet. The system was solvated with 25,471 waters, 102 sodiums, and 42 chlorides. The hydration level was chosen to accommodate the Anton box length requirements. The system was equilibrated for 100 ns on LoBoS, and then simulated for 1 μ s on Anton. The simulation was then heated to 413 with a -0.2 V applied electric field (the same as in Article I) for 20 ns, and run for another 1 μ s on Anton. Application of an electric field on Anton is described in Jensen et al. (47).

Preparation of samples for ssNMR

Oriented samples were prepared following a protocol previously reported in Chekmenev et al. (48). Briefly, HPLC-purified p1 and the lipids (Avanti Polar Lipids, Alabaster, AL) were codissolved in chloroform and 2,2,2-trifluoroethanol (Fisher Scientific, Pittsburgh, PA) to reach a

TABLE 1 Summary of Simulations Reported Here

Simulation	Temp (K)	E-field (mV)	Time (μ s)	Primary Result
Twenty peptides starting as pores				
Initial pore (IP ₀)	313	0.0	26	Eighteen of 20 peptides become surface-bound
Continued from IP ₂₅ ^a	313	0.0	3×0.25	
Continued from IP ₂₅	313	-0.2	0.18	No change
Continued from IP ₂₅	413	-0.2	0.04	Bilayer unstable
Continued from IP ₂₅	413	0.2	0.16	Last two peptides diffuse to surface
Started from IP ₀	413	-0.2	0.05	All peptides become surface-bound
Started from IP ₀	413	0.2	0.23	All peptides become surface-bound
Sixteen peptides starting from the surface of both leaflets (eight per leaflet)				
Initial surface	313	0.0	2.8	Peptides helical, no insertion, defects
Ten peptides starting on the surface of one leaflet				
Initial surface	313	0.0	1	Peptides helical, no insertion, defects
Continued from initial surface	313	-0.2	1	Peptides helical, no insertion, defects
Continued from initial surface	413	-0.2	1	Peptides helical, no insertion, defects

^aIP₂₅ refers to the 25- μ s coordinate set of the initial pore system (IP₀).

^aThree replicas initialized with new velocities.

peptide/lipid molar ratio of 1:12 and a POPC/POPG molar ratio of 3:1. After evaporating the organic solvents, the samples were placed under vacuum overnight to dry thoroughly. The peptide/lipid films were then hydrated overnight using 3 mM phosphate buffer at pH 7.4 and 37°C. After centrifugation as needed to remove excess hydration, the samples were spread on thin glass slides (dimensions $5.7 \times 12 \times 0.03 \text{ mm}^3$ from Matsunami Trading, Osaka, Japan) and placed in a chamber in the presence of a saturated solution of K_2SO_4 to achieve a relative humidity $>90\%$. Additional buffer was added to the slides as needed to reach a hydration level of at least 40% by weight. Once stacked, the slides were transferred to a glass cell (VetroCom, Kyoto, NJ) that was sealed using beeswax, and incubated at 37°C until homogeneous hydration was reached.

ssNMR experiments

The ^{15}N ssNMR measurements were carried out on a Bruker Avance 600 NMR spectrometer, where ^{15}N and ^1H Larmor frequencies were 60.81 and 600.13 MHz, respectively. A homebuilt low-electrical field wide-line ^1H - ^{15}N double-resonance NMR probe with a flat sample coil was used to minimize the sample heating due to the radio-frequency (RF) irradiation during the NMR measurements. The ^{15}N signals were enhanced with the frequency modulated cross-polarization (CP) scheme (49,50). Specifically, the ^{15}N carrier frequency was modulated by a single cycle of a sine wave while its RF amplitude was kept constant over the CP contact time during which the ^1H magnetization was spin-locked in the xy plane. The depth of the ^{15}N frequency modulation was 40 kHz with the RF amplitude of 40 kHz while the ^1H RF amplitude was 50 kHz during the CP contact time of 1 ms. Thus, all ^{15}N signals could be effectively enhanced over a large spectral width ($\sim \pm 30$ kHz, corresponding to ± 493 ppm centered at the carrier frequency of 76.4 ppm). During acquisition, the ^{15}N signals were recorded under a high power SPINAL64 ^1H decoupling (51) at an RF amplitude of 62 kHz. The ^{15}N chemical shift was referenced to 0 ppm using a saturated solution of $(^{15}\text{NH}_4)_2\text{SO}_4$.

The ^{31}P solid-state NMR data were recorded using a spin echo sequence on a 400 MHz NMR magnet equipped with a Bruker DRX console. Experiments were performed at the Larmor frequencies of 162.12 MHz for ^{31}P and 400.49 MHz for ^1H on a homebuilt wide-line ^1H - ^{31}P double-resonance probe with a flat coil. The ^{31}P 90°-pulse length used was 5 μs and the echo time was 30 μs . A SPINAL64 sequence with the RF amplitude of 62 kHz was used for ^1H decoupling during the ^{31}P acquisition. The ^{31}P chemical shift was referenced to a H_3PO_4 solution at 0 ppm.

The sample temperatures for the ^{15}N and the ^{31}P NMR measurements were regulated by a BVT-2000 unit (Bruker) with a precision of ± 0.1 K.

RESULTS AND DISCUSSION

Just as for Article I, Table 1 contains a list of simulations, the conditions, and the primary result from each.

The 26 μs trajectory of p1 pores

Peptides become surface-bound

All four p1 pores (Fig. 1 a) converted to toroidal by 0.2 μs (Fig. 1 b); the recruitment of both POPG (purple) and POPC (gray) lipid headgroups into the membrane interior is evident. The top time series in Fig. 1 plots the fraction of S peptides over the course of 26 μs . The trajectory has four regions with apparently stable fractions of S peptides (white background), and four transitional regions (orange background). Transitional regions are characterized by a large increase in fraction of S and decrease in the number

of pore waters and pore lipids (middle and bottom time series of Fig. 1). Waters are defined as being in a pore if they are within 10 Å of the bilayer midplane and 20 Å from the center of the pore in the xy plane; lipids are considered part of the pore if their phosphates meet the preceding criteria. Each pore lost at least one peptide in the first 5 μs , resulting in 12 S peptides and a subpopulation of T peptides (Fig. S1 b). The following 5 μs involved transitions between the T and S orientations (Fig. S2), but the average number of S peptides remained at 12. Fig. 1 b is a snapshot of the simulation at 10 μs . Three porelike structures remained: two pores contained multiple TM peptides, while the third consisted of one peptide and a disrupted water channel. Transition of this remaining peptide to a S orientation initiated the next disruptive period, followed by 3 μs of two pores, one of which is lost at 15 μs . The remaining two-peptide (parallel) pore was stable for the last 5 μs ; Fig. 1 c shows the last frame of the trajectory.

Pore properties and assessing stability

Among the pores in the 26 μs simulation, each inserted peptide is accompanied by ~ 20 waters and two lipids (Fig. S3). Of the pore lipids, POPG/POPC is ~ 2 and the root mean-squared fluctuation is 1 (Fig. S3). Considering the 3:1 of POPC/POPG in the entire system, the preference of POPG in a pore is then $\sim 6:1$. This preference for an anionic lipid reduces the net charge at the center of the pore. The one pore that remains in the final 10 μs contains two peptides (net charge of $+4e$ per peptide), four POPGs (net charge of $-1e$ per lipid) and one POPC, 40 waters, and no ions. The net charge for the peptide-lipid pore is therefore $+4e$. Lipid flip-flop was mediated by the pores, and after 26 μs , 32 of the 200 lipids exchanged leaflets (19 were POPGs).

Given the observation that the other three pores dissociated, and that no peptides reinserted, one may plausibly infer that the remaining pore will also dissociate. However, limitations of computer time (26 μs approximately equaled a yearly Anton allocation for a system of this size at the time of the simulations) did not permit an explicit demonstration of instability. Furthermore, numerous long replicate simulations would provide a more convincing test of the hypothesis that the pore state is unstable.

Consequently, additional trajectories, some at higher temperatures and applied electric fields, were generated to explore the stability of the porelike assembly. These are listed in Table 1. Most were started with the 25 μs coordinate set (denoted IP₂₅) from the 26- μs initial pore simulation described above. Three were restarted at 313 K with new velocities and run for 250 ns. The deviation between replicas was small, and the pore remained intact. Next, a 180 ns simulation was carried out at 313 K with an applied electric field of -0.2 V. As before, the pore assembly remained intact. Next, a trajectory was run at 413 K

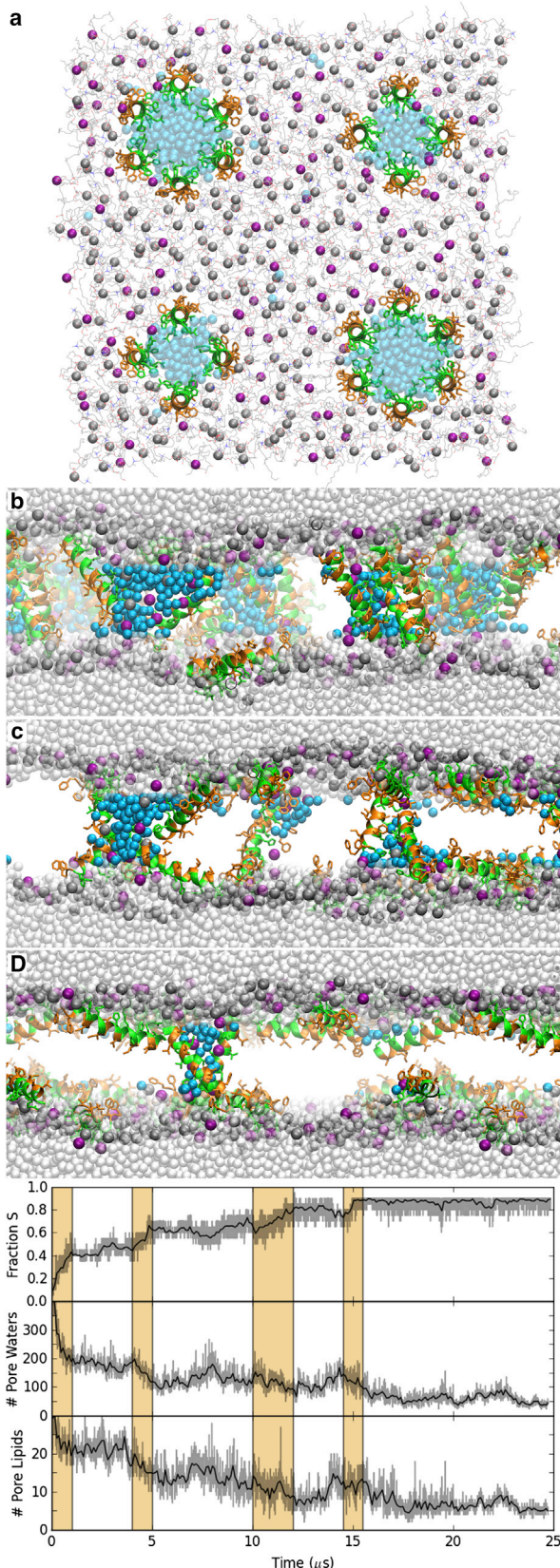


FIGURE 1 (a) Initial conditions for the 26 μs simulation of p1. The length of the system is 126.3 \AA in the x - and y dimensions and 85.0 \AA in the z dimension. Snapshots of the 26 μs simulation at 0.2 (b), 10 (c), and

with a -0.2 V external electric field. This condition led to insertion of alamethicin peptides in Article I (35); however, here the system became unstable. When the orientation of the electric field was reversed, however, the bilayer remained stable and the pore disassociated after 35 ns. For the final two simulations, the initial pore construction (IP_0) was simulated at 413 K with a -0.2 or $+0.2$ V external electric field. All peptides became surface-bound within 50 ns for -0.2 V and 230 ns for $+0.2$ V. These results imply that the pore assemblies of piscidin are indeed unstable at room temperature, and indicate that a rigorous enhanced sampling procedure will be required to show this conclusively with simulation alone.

Peptide secondary structure

The peptides remained highly α -helical throughout the simulation. In four of the 20 peptides, the first three residues frayed supporting the previous observation that the N-terminal residues are the most disordered (30). This fraying is more pronounced for TM peptides, which were observed to transiently unravel their first three N-terminal residues to partition the phenylalanines in the hydrocarbon core before reaching the interface and refolding into an α -helical secondary structure. As already noted, p1 contains a kink. This kink, which is formed by a relative rotation of the α -helical segments on either side of the central glycine 13 (termed $\Delta\rho$), does not bend the helix and has been proposed to stabilize the S state by maximizing the hydrophobic moment of the helix (30). As shown in Fig. 2, the average $\Delta\rho$ is comparable in the S and TM states ($\approx 20^\circ$), but the root mean-squared fluctuations are three times higher in the latter (24 vs. 8°). Hence, the kink loses much of its rigidity when the peptide becomes TM.

Surface-bound simulation shows nonpore defects

A 2.8 μs simulation of 16 surface-bound peptides with 320 lipids and 56 waters per lipid (performed on a local cluster) explored the dynamics of p1 unperturbed by a TM starting orientation. The peptides remain in S throughout the simulation, with average structures in agreement with those previously simulated and studied by high resolution ssNMR (30). After 0.8 μs , the first of a series of transient defects formed in the bilayer. In each instance where a defect developed, several peptides inserted one end deep into the bilayer, taking on a tilted conformation (Fig. 3, top), and then

26 μs (d). Peptides are colored by residue type (orange for hydrophobic residues; polar and charged (green), waters within 10 \AA of the midplane (cyan), POPC phosphates (gray), and POPG phosphates (purple) are also displayed. (Bottom) Fractional composition of surface-bound (S) peptide (top), pore waters (middle), and pore lipids (bottom) averaged over 100 ns blocks. Areas with an orange background represent times of significant changes in the fraction of S.

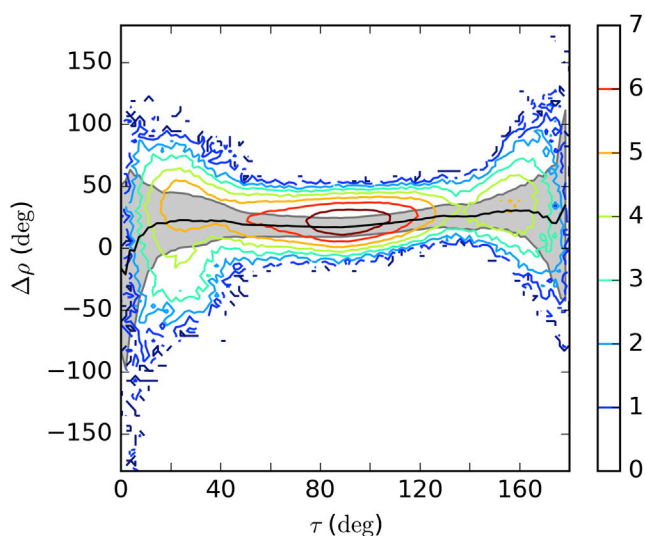


FIGURE 2 Contour plot of peptide tilt (τ) versus kink about the helical axis ($\Delta\rho$) for all peptides in the 26- μ s simulation (contours represent the natural log of the count density), along with the average $\Delta\rho$ (solid black line) and root-mean squared fluctuation (gray lines and shading).

returned to the more usual S orientations after 10–30 ns. These events coincided with a decrease in the membrane surface area, an increase in large membrane undulations, and formation of substantial funnel of water (>50 water molecules within 10 Å of the midplane). Single water molecules traversed the membrane from this funnel; however, a

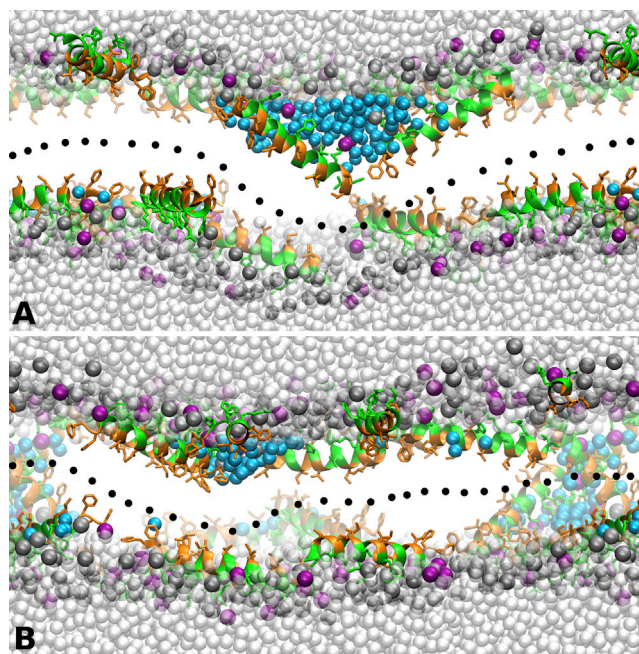


FIGURE 3 Snapshots illustrating insertion of a surface-bound peptide in simulations started from surface-bound (A) and pore (B) orientations at 0.9 and 19.8 μ s, respectively. The same coloring scheme as in Fig. 1 is used. (Dotted lines) Midplane.

continuous channel was never formed. The peptides did not become TM because the opposing leaflet bulged away to compensate (dashed lines in Fig. 3, top). Similar insertion events were observed in the 26- μ s simulation after most of the pores had dissipated (Fig. 3, bottom). Fig. S4 plots the time series for the z coordinate of the N- and C-terminal C α averaged in 10-ns blocks for the 2.8- μ s surface-bound simulation. Five C-terminal crossings of the midplane and one N-terminal crossing were observed, indicating a preference for deep insertion of the C-terminus as the defect formed. Moreover, the distribution of peptide orientations in the surface-bound simulation (Fig. S1 d) is comparable to that of the nonpore peptides in the last 10 μ s of the 26 μ s simulation (Fig. S1 c). Among all S peptides in both simulations, the α -carbon of the N-terminal residue is \sim 3 Å deeper than that of the C-terminal residue, but the C-terminus fluctuates over a broader range (Fig. S1).

Simulations of piscidin on only one leaflet were also performed to test that the potential for insertion of only one leaflet was influenced by peptide. After 1 μ s, the peptides remained surface-bound and α -helical. The similarity between the surface-bound peptides in the last 10 μ s of the 26 μ s simulation and the 2.8- μ s surface-bound simulation indicated that a single microsecond was sufficient. In contrast, the first microsecond of a 5- μ s alamethicin simulation from Article I demonstrated significant peptide unfolding and unbinding from the membrane surface, which supported extending that simulation. Moreover, heating the system to 413 K and adding a -0.2 V electric field accelerated the insertion of surface-bound alamethicin. The same conditions were applied to the piscidin simulation for 1 μ s. While the distribution of peptide tilts and the frequency of defects increased with heat and an electric field, peptide insertion was not observed.

TM states not observed by oriented sample ssNMR

Fig. 4 (top) shows ssNMR spectra for 15 N-labeled V10 p1 in hydrated 3:1 POPC/POPG bilayers aligned on glass plates at a P/L of 1:12 and pH 7.4. At 305 K, well above the phase transition temperature of the lipids (271 K), the TM state was not observed even though the peptide concentration was well above the amount needed to permeabilize the membrane (28,29). Additional measurements were taken at the lower temperatures of 285 and 278 K to explore the possibility that the TM to S states are in fast exchange and a lower temperature could help trap them. In all cases, the spectra show a single peak at 50 ppm indicative of a surface-bound peptide (2), which is similar to the results previously obtained at a P/L of 1:20 (30). There is no signal in the region expected for TM orientations (\sim 180–200 ppm for TM helices with orientations varying between 0 and 15° with respect to the bilayer normal (52)).

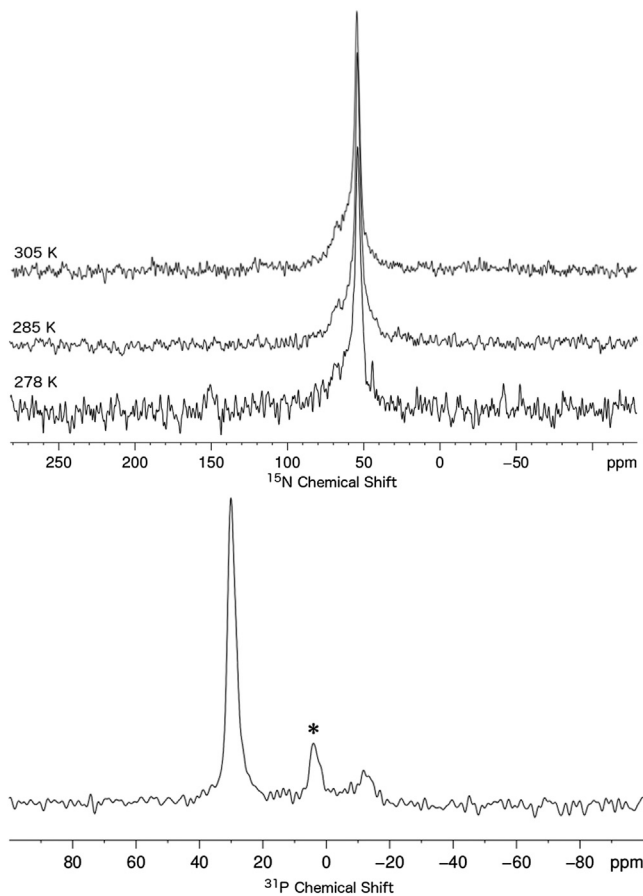


FIGURE 4 (Top) Solid-state NMR spectra of ^{15}N -Val $_{10}$ p1 in hydrated oriented 3:1 POPC/POPG bilayers at 278, 280, and 305 K at a P/L of 1:12 and pH 7.4 (phosphate buffer). (Bottom) ^{31}P ss NMR spectrum of the same sample as in above recorded at 305 K. For all spectra, the bilayer normal was oriented parallel to the magnetic field; an asterisk (*) marks the phosphate buffer signal.

The alignment of the lipids with respect to the bilayer normal was assessed using the ^{31}P -oriented chemical shift spectrum of the same sample containing ^{15}N -V10 p1 (Fig. 4, bottom). In an unoriented sample (i.e., no glass plates), the spectrum would span the range of chemical shifts between -16 and 30 ppm. The spectrum recorded with the bilayer normal parallel to the magnetic field displays three peaks: the largest at 30 ppm is indicative of lipid molecules aligned parallel to the bilayer normal as expected in a sample aligned on glass plates, the middle at 4 ppm is the phosphate buffer, and the smallest at -15 ppm is from lipids oriented perpendicular to the bilayer normal as predicted for lipids lining toroidal pores. The lipid area for the peak at -16 ppm is $11 \pm 3\%$ of the total lipid area. However, this region of the spectrum also includes signals from lipids that could be on the edge of the glass plates creating a mosaic spread, or lipids perturbed by S-state peptides as seen in the MD simulations (which appears to be significant for the tilted peptides in Fig. 3). Overall, both

MD and NMR indicate a low population of peptides and lipids with features of toroidal pores.

CONCLUSIONS

The central result of this study comes from the $26 \mu\text{s}$ simulation: p1 does not form stable pores in any appreciable concentration in 3:1 POPC/POPG bilayers at full hydration. As Fig. 1 shows, the initial barrel-stave pores rapidly became toroidal, and then, in several time periods, all but two of the peptides migrated from their TM to S orientations. While the barrel-stave structures were not expected to be stable, the TM orientations provided excellent starting points for forming and equilibrating disordered toroidal pores. Despite the pore lifetimes of 5 – $26 \mu\text{s}$, the pore peptides and lipids were unable to pack favorably or recruit surface peptides. This is further demonstrated by the absence of peptide transitions from S to TM under all conditions, and the rapid breakdown of the pores at high temperature with an applied electric field. This low probability of pores is corroborated by the ^{15}N and ^{31}P measurements presented here (Fig. 4). In contrast to the simulations that were heated to increase sampling, the ^{15}N chemical shifts were measured at low temperatures to trap the inserted state. Despite these efforts, only S peptides were measurable. These results suggest that the conductance (28), dye leakage (26,29), and ssNMR (32) studies noted earlier should be reinterpreted to include the possibility of a nonpore mechanism for piscidin.

While these simulations do not unambiguously reveal a nonpore disruption mechanism for p1, they do provide some support for the interfacial activity and charge clustering models. The surface-bound peptides induce transient defects that cause water permeation without forming stable pores or substantially remodeling the membrane (Fig. 3) similar to the interfacial activity model. The most tilted peptide orientations are associated with water permeation, as well as bulging of the opposing leaflet that interrupts translocation. Charge clustering was observed by the preference for POPG in the transient toroidal pores. These anionic lipids stabilized the pores and mediated peptide translocation. However, the ^{31}P chemical shift spectra indicate that such peptide-lipid complexes could only be present in very low concentrations.

The alamethicin simulations in Article I and the p1 simulations described here are contrasting examples of membrane-disrupting peptides with barrel-stave pore and nonpore mechanisms. What makes them different? Both have potentially stable amphipathic α -helical structures; however, alamethicin is significantly more hydrophobic. Both peptides also have central kinks. The central proline of alamethicin forms a kink that disrupts the helix, and is proposed to stabilize the pores (53,54). In contrast, the glycine-associated kink in p1 provides flexibility, maintains

the linearity of the helix, and increases the μH to 6.0 kcal/mol (an increase of 4%) (30). The types and positions of aromatic residues of the peptides are also different. The one phenylalanine in alamethicin is the terminal residue in the disordered peptide segment and is buried in the membrane without disrupting the pore. Piscidin 1 has three phenylalanines in the N-terminal segment securing it in the bilayer while the C-terminal samples a wide range of depths (Fig. S1 d). The insertions of the C-terminal segment to the bilayer midplane lead to defects (Fig. 3), which are potential precursors to piscidin's disruption mechanism. These features of p1 (straight helix, large hydrophobic moment, well-positioned aromatic residues, and ability to flex at a central glycine and to tilt) strongly stabilize its surface-bound state. In contrast, as discussed in Article I, the surface-bound alamethicin lost helicity and only weakly binds to the bilayer surface; i.e., the small polar angle of alamethicin (Article I, Fig. 1) that correlates with the barrel stave pore appears to destabilize the S-state.

Simulations of the pore states reveal substantial differences in the helical structures and positioning of charged residues between the two peptides. Alamethicin lost half of its α -helical content (in agreement with experiment), but the peptides remained TM and formed a stable water channel with a single charged residue/peptide (E18) at the surface. The N-terminal residues of p1 unraveled to bury the phenylalanines in the bilayer interior and the glycine kink lost its rigidity (Fig. 2); however, three charged residues/peptide (R7, K14, and R18) remained in the (unstable) pores. While these residues are partially neutralized by POPG headgroups, the high charge density of p1 pores likely destabilizes them with respect to alamethicin. The simulations also provided more direct evidence of stability: alamethicin reincorporated a S-peptide into the pore. In contrast, there was not a single instance of recruitment of a S-peptide to a pore in the simulations of p1.

In conclusion, it is critical to understand the differences in the membrane active states of alamethicin and p1 in terms of a balance of stability of the surface-bound and inserted conformations of each peptide. It appears that the antimicrobial peptide p1 and likely other AMPs, has evolved to strongly favor the surface-bound state over the pore state. The multimicrosecond simulations presented in Article I and here illustrate the long simulation timescales necessary for addressing stability of peptide-stabilized pores. However, the insertion of alamethicin in Article I, and the piscidin surface defects provide clues to accelerated simulation techniques that can circumvent inaccessible timescales.

SUPPORTING MATERIAL

Supporting Materials and Methods and four figures are available at [http://www.biophysj.org/biophysj/supplemental/S0006-3495\(16\)30703-2](http://www.biophysj.org/biophysj/supplemental/S0006-3495(16)30703-2).

AUTHOR CONTRIBUTIONS

B.S.P., M.L.C., and R.W.P. designed the research; B.S.P. carried out the simulations; M.L.C. and R.F. carried out the NMR experiments; and B.S.P. and R.W.P. wrote the article with help from M.L.C. and R.F.

ACKNOWLEDGMENTS

The Anton machine at the Pittsburgh Supercomputing Center was generously made available by D. E. Shaw Research.

This research was supported in part by the Intramural Research Program of the National Institutes of Health, National Heart, Lung and Blood Institute, the National Science Foundation CAREER grant award (No. CHE 0832571), and a Dreyfus Foundation grant, and utilized the high performance computational capabilities at the National Institutes of Health, Bethesda, MD (National Heart, Lung and Blood Institute LoBoS cluster). Anton computer time was provided by the National Center for Multiscale Modeling of Biological Systems through grant No. P41GM103712-S1 from the National Institutes of Health and the Pittsburgh Supercomputing Center. The NMR experiments were performed at the National High Magnetic Field Lab supported by National Science Foundation Cooperative Agreement No. DMR-1157490 and the State of Florida.

REFERENCES

- Jenssen, H., P. Hamill, and R. E. W. Hancock. 2006. Peptide antimicrobial agents. *Clin. Microbiol. Rev.* 19:491–511.
- Bechinger, B., M. Zasloff, and S. J. Opella. 1993. Structure and orientation of the antibiotic peptide magainin in membranes by solid-state nuclear magnetic resonance spectroscopy. *Protein Sci.* 2:2077–2084.
- Nicolas, P. 2009. Multifunctional host defense peptides: intracellular-targeting antimicrobial peptides. *FEBS J.* 276:6483–6496.
- Hilchie, A. L., K. Wuerth, and R. E. W. Hancock. 2013. Immune modulation by multifaceted cationic host defense (antimicrobial) peptides. *Nat. Chem. Biol.* 9:761–768.
- Wimley, W. C., and K. Hristova. 2011. Antimicrobial peptides: successes, challenges and unanswered questions. *J. Membr. Biol.* 239:27–34.
- Yang, L., T. A. Harroun, ..., H. W. Huang. 2001. Barrel-stave model or toroidal model? A case study on melittin pores. *Biophys. J.* 81:1475–1485.
- Pan, J., S. Tristram-Nagle, and J. F. Nagle. 2009. Alamethicin aggregation in lipid membranes. *J. Membr. Biol.* 231:11–27.
- He, K., S. J. Ludtke, ..., H. W. Huang. 1996. Neutron scattering in the plane of membranes: structure of alamethicin pores. *Biophys. J.* 70:2659–2666.
- He, K., S. J. Ludtke, ..., D. L. Worcester. 1995. Antimicrobial peptide pores in membranes detected by neutron in-plane scattering. *Biochemistry.* 34:15614–15618.
- Qian, S., W. Wang, ..., H. W. Huang. 2008. Structure of the alamethicin pore reconstructed by x-ray diffraction analysis. *Biophys. J.* 94:3512–3522.
- Lee, M.-T., F.-Y. Chen, and H. W. Huang. 2004. Energetics of pore formation induced by membrane active peptides. *Biochemistry.* 43:3590–3599.
- Song, C., C. Weichbrodt, ..., K. Zeth. 2013. Crystal structure and functional mechanism of a human antimicrobial membrane channel. *Proc. Natl. Acad. Sci. USA.* 110:4586–4591.
- Uematsu, N., and K. Matsuzaki. 2000. Polar angle as a determinant of amphipathic α -helix-lipid interactions: a model peptide study. *Biophys. J.* 79:2075–2083.
- Bertelsen, K., J. Dorosz, ..., T. Vosegaard. 2012. Mechanisms of peptide-induced pore formation in lipid bilayers investigated by oriented ^{31}P solid-state NMR spectroscopy. *PLoS One.* 7:e47745.

15. Leveritt, J. M., 3rd, A. Pino-Angeles, and T. Lazaridis. 2015. The structure of a melittin-stabilized pore. *Biophys. J.* 108:2424–2426.
16. Allende, D., S. A. Simon, and T. J. McIntosh. 2005. Melittin-induced bilayer leakage depends on lipid material properties: evidence for toroidal pores. *Biophys. J.* 88:1828–1837.
17. Sengupta, D., H. Leontiadou, ..., S.-J. Marrink. 2008. Toroidal pores formed by antimicrobial peptides show significant disorder. *Biochim. Biophys. Acta.* 1778:2308–2317.
18. Strandberg, E., and A. S. Ulrich. 2015. AMPs and OMPs: is the folding and bilayer insertion of β -stranded outer membrane proteins governed by the same biophysical principles as for α -helical antimicrobial peptides? *Biochim. Biophys. Acta.* 1848:1944–1954.
19. Krauson, A. J., J. He, and W. C. Wimley. 2012. Determining the mechanism of membrane permeabilizing peptides: identification of potent, equilibrium pore-formers. *Biochim. Biophys. Acta.* 1818:1625–1632.
20. Epanand, R. F., W. L. Maloy, ..., R. M. Epanand. 2010. Probing the “charge cluster mechanism” in amphipathic helical cationic antimicrobial peptides. *Biochemistry.* 49:4076–4084.
21. Wimley, W. C. 2010. Describing the mechanism of antimicrobial peptide action with the interfacial activity model. *ACS Chem. Biol.* 5:905–917.
22. Hristova, K., M. E. Selsted, and S. H. White. 1997. Critical role of lipid composition in membrane permeabilization by rabbit neutrophil defensins. *J. Biol. Chem.* 272:24224–24233.
23. Gazit, E., I. R. Miller, ..., Y. Shai. 1996. Structure and orientation of the mammalian antibacterial peptide cecropin P1 within phospholipid membranes. *J. Mol. Biol.* 258:860–870.
24. Menousek, J., B. Mishra, ..., G. Wang. 2012. Database screening and in vivo efficacy of antimicrobial peptides against methicillin-resistant *Staphylococcus aureus* USA300. *Int. J. Antimicrob. Agents.* 39:402–406.
25. Wang, G., K. M. Watson, ..., R. W. Buckheit, Jr. 2010. Identification of novel human immunodeficiency virus type 1-inhibitory peptides based on the antimicrobial peptide database. *Antimicrob. Agents Chemother.* 54:1343–1346.
26. Sung, W. S., J. Lee, and D. G. Lee. 2008. Fungicidal effect of piscidin on *Candida albicans*: pore formation in lipid vesicles and activity in fungal membranes. *Biol. Pharm. Bull.* 31:1906–1910.
27. Lin, H.-J., T.-C. Huang, ..., C.-H. Lin. 2012. Piscidin-1, an antimicrobial peptide from fish (hybrid striped bass *Morone saxatilis* x *M. chrysops*), induces apoptotic and necrotic activity in HT1080 cells. *Zoolog. Sci.* 29:327–332.
28. Campagna, S., N. Saint, ..., A. Aumelas. 2007. Structure and mechanism of action of the antimicrobial peptide piscidin. *Biochemistry.* 46:1771–1778.
29. Lee, S.-A., Y. K. Kim, ..., Y. Kim. 2007. Solution structure and cell selectivity of piscidin 1 and its analogues. *Biochemistry.* 46:3653–3663.
30. Perrin, B. S., Jr., Y. Tian, ..., M. L. Cotten. 2014. High-resolution structures and orientations of antimicrobial peptides piscidin 1 and piscidin 3 in fluid bilayers reveal tilting, kinking, and bilayer immersion. *J. Am. Chem. Soc.* 136:3491–3504.
31. Perrin, B. S., Jr., A. J. Sodt, ..., R. W. Pastor. 2014. The curvature induction of surface-bound antimicrobial peptides piscidin 1 and piscidin 3 varies with lipid chain length. *J. Membr. Biol.* 248:455–467.
32. De Angelis, A. A., C. V. Grant, ..., M. L. Cotten. 2011. Amphipathic antimicrobial piscidin in magnetically aligned lipid bilayers. *Biophys. J.* 101:1086–1094.
33. Fantner, G. E., R. J. Barbero, ..., A. M. Belcher. 2010. Kinetics of antimicrobial peptide activity measured on individual bacterial cells using high-speed atomic force microscopy. *Nat. Nanotechnol.* 5:280–285.
34. Shaw, D. E., R. O. Dror, ..., B. Towles. 2009. Millisecond-scale molecular dynamics simulations on Anton. In Proceedings of the Conference on High Performance Computing Networking, Storage and Analysis. ACM, Portland, Oregon, pp. 1–11.
35. Perrin, B. S., Jr., and R. W. Pastor. 2016. Simulations of membrane-disrupting peptides I: alamethicin pore stability and spontaneous insertion. *Biophys. J.* 111:1248–1257.
36. Hoover, W. G. 1985. Canonical dynamics: equilibrium phase-space distributions. *Phys. Rev. A Gen. Phys.* 31:1695–1697.
37. Nosé, S. 1984. A unified formulation of the constant temperature molecular-dynamics methods. *J. Chem. Phys.* 81:511–519.
38. Nosé, S., M. L. Klein, and S. Nosé. 1983. A study of solid and liquid carbon tetrafluoride using the constant pressure molecular dynamics technique. *J. Chem. Phys.* 78:6928.
39. Andersen, H. C. 1980. Molecular dynamics simulations at constant pressure and/or temperature. *J. Chem. Phys.* 72:2384.
40. Brooks, B. R., C. L. Brooks III, ..., M. Karplus. 2009. CHARMM: the biomolecular simulation program. *J. Comput. Chem.* 30:1545–1614.
41. Martyna, G. J., D. J. Tobias, and M. L. Klein. 1994. Constant pressure molecular dynamics algorithms. *J. Chem. Phys.* 101:4177–4189.
42. MacKerell, A. D., D. Bashford, ..., M. Karplus. 1998. All-atom empirical potential for molecular modeling and dynamics studies of proteins. *J. Phys. Chem. B.* 102:3586–3616.
43. Klauda, J. B., R. M. Venable, ..., R. W. Pastor. 2010. Update of the CHARMM all-atom additive force field for lipids: validation on six lipid types. *J. Phys. Chem. B.* 114:7830–7843.
44. Venable, R. M., A. J. Sodt, ..., J. B. Klauda. 2014. CHARMM all-atom additive force field for sphingomyelin: elucidation of hydrogen bonding and of positive curvature. *Biophys. J.* 107:134–145.
45. Jo, S., T. Kim, ..., W. Im. 2008. CHARMM-GUI: a web-based graphical user interface for CHARMM. *J. Comput. Chem.* 29:1859–1865.
46. Fox, R. O., Jr., and F. M. Richards. 1982. A voltage-gated ion channel model inferred from the crystal structure of alamethicin at 1.5-Å resolution. *Nature.* 300:325–330.
47. Jensen, M. Ø., V. Jogini, ..., D. E. Shaw. 2013. Atomic-level simulation of current-voltage relationships in single-file ion channels. *J. Gen. Physiol.* 141:619–632.
48. Chekmenev, E. Y., S. M. Jones, ..., M. Cotten. 2006. High-field NMR studies of molecular recognition and structure-function relationships in antimicrobial piscidins at the water-lipid bilayer interface. *J. Am. Chem. Soc.* 128:5308–5309.
49. Fu, R., P. Pelupessy, and G. Bodenhausen. 1997. Frequency-modulated cross-polarization for fast magic angle spinning NMR at high fields: relaxing the Hartmann-Hahn condition. *Chem. Phys. Lett.* 264:63–69.
50. Kim, H., T. A. Cross, and R. Fu. 2004. Cross-polarization schemes for peptide samples oriented in hydrated phospholipid bilayers. *J. Magn. Reson.* 168:147–152.
51. Fung, B. M., A. K. Khitritin, and K. Ermolaev. 2000. An improved broadband decoupling sequence for liquid crystals and solids. *J. Magn. Reson.* 142:97–101.
52. Wang, J., J. Denny, ..., T. A. Cross. 2000. Imaging membrane protein helical wheels. *J. Magn. Reson.* 144:162–167.
53. Kaduk, C., H. Duclouhier, ..., M. Bienert. 1997. Influence of proline position upon the ion channel activity of alamethicin. *Biophys. J.* 72:2151–2159.
54. Krauson, A. J., J. He, and W. C. Wimley. 2012. Gain-of-function analogues of the pore-forming peptide melittin selected by orthogonal high-throughput screening. *J. Am. Chem. Soc.* 134:12732–12741.